



## Mesoscale variability related to iron speciation in a coastal Ross Sea area (Antarctica) during summer 2014

Paola Rivaro, Francisco Ardini, Marco Grotti, Giuseppe Aulicino, Yuri Cotroneo, Giannetta Fusco, Olga Mangoni, Francesco Bolinesi, Maria Saggiomo & Mauro Celussi

To cite this article: Paola Rivaro, Francisco Ardini, Marco Grotti, Giuseppe Aulicino, Yuri Cotroneo, Giannetta Fusco, Olga Mangoni, Francesco Bolinesi, Maria Saggiomo & Mauro Celussi (2019) Mesoscale variability related to iron speciation in a coastal Ross Sea area (Antarctica) during summer 2014, *Chemistry and Ecology*, 35:1, 1-19, DOI: [10.1080/02757540.2018.1531987](https://doi.org/10.1080/02757540.2018.1531987)

To link to this article: <https://doi.org/10.1080/02757540.2018.1531987>



Published online: 11 Oct 2018.



Submit your article to this journal [↗](#)



Article views: 73



View related articles [↗](#)











View Crossmark data [↗](#)

RESEARCH ARTICLE



## Mesoscale variability related to iron speciation in a coastal Ross Sea area (Antarctica) during summer 2014

Paola Rivaro <sup>a</sup>, Francisco Ardini <sup>a</sup>, Marco Grotti <sup>a</sup>, Giuseppe Aulicino <sup>b,f</sup>, Yuri Cotroneo <sup>b</sup>, Giannetta Fusco <sup>b</sup>, Olga Mangoni <sup>c</sup>, Francesco Bolinesi<sup>c</sup>, Maria Saggiomo<sup>d</sup> and Mauro Celussi <sup>e</sup>

<sup>a</sup>Department of Chemistry and Industrial Chemistry, University of Genoa, Genoa, Italy; <sup>b</sup>Department of Science and Technology, Parthenope University of Naples, Naples, Italy; <sup>c</sup>Department of Biology, University of Napoli Federico II, Naples, Italy; <sup>d</sup>Stazione Zoologica Anton Dohrn, Naples, Italy; <sup>e</sup>OGS (Istituto Nazionale di Oceanografia e Geofisica Sperimentale), Oceanography Division, Trieste, Italy; <sup>f</sup>Department of Life and Environmental Sciences, Marche Polytechnic University, Ancona, Italy

### ABSTRACT

Dissolved iron (Fe) distribution and speciation was determined in water samples (0–200 m) collected in a coastal area near Terra Nova Bay during the austral summer of 2014. Nutrients, dissolved oxygen, chlorophyll-a, phytoplankton composition and prokaryotic biomass distribution were investigated in combination with measurements of the physical properties of the water columns and its dynamics. The dFe value was above the limiting growth concentration, ranging from 0.52 to 4.51 nM, and it showed a spatial variability with a horizontal length scale of about 10 km, according to the variability of the water column physical properties and to iron sources. The organic ligands (L) maintained the concentrations of dFe at levels much higher than the inorganic solubility of Fe, keeping it available for phytoplankton and the  $\log K'_{\text{FeL}}$  values found (from 22.1 to 23.6) highlighted the presence of complexes of differing stabilities.

### ARTICLE HISTORY

Received 17 May 2018  
Final Version Received  
1 October 2018

### KEYWORDS

Ross Sea; mesoscale;  
dissolved iron; iron  
speciation; biological activity;  
Antarctica

## 1. Introduction

Iron (Fe) is the most important trace metal in the ocean, being involved in several metabolic pathways, including biosynthesis of chlorophyll, transport of electrons through the photosynthetic and respiratory transport chains and nitrate assimilation by phytoplankton [1,2]. In the Southern Ocean, which is strongly characterised by mesoscale activity [3,4] and intense interactions between sea surface and atmosphere [5–7], iron supply influences phytoplankton biomass and species composition, as well as primary productivity in both high and low nitrate surface waters [8,9]. The quantum yield ( $F_v/F_m$ ) of phytoplankton is Fe-driven and low values should be indicators of Fe stress [10,11]. Moreover, Fe is also used over the whole water column by microbial communities which are responsible for the degradation and remineralisation of sinking organic matter [12]. Fe is present in

seawater in different physical (particulate, colloidal, dissolved) and chemical (inorganic and organic complexes) forms. It has been recognised that Fe bioavailability is influenced by the chemical forms, biogeochemical cycling and the different uptake strategies of the phytoplankton and bacterioplankton communities [13]. Despite the dissolved Fe (dFe) concentrations in the ocean being extremely low, they are higher than might be calculated on the basis of the solubility of ferric hydroxide in seawater at pH 8.1 and 25°C due to the ability of iron to form organic complexes [14]. Oceanographic research has shown that more than 99% of the dFe in the ocean is bound to organic ligands [15]. It is now widely recognised that, in high-nutrient low-chlorophyll (HNLC) regions, the algal growth is limited, not only by a general lack of Fe, but also by the bioavailability of organically bound Fe [16–19]. The Ross Sea accounts for almost 30% of the total Southern Ocean annual production [20]. Significant inter-annual variability in phytoplankton biomass has been observed and substantial rates of primary production ( $>1 \text{ g C m}^{-2} \text{ d}^{-1}$ ) are often associated in the shelf area with polynyas, fronts and marginal ice zones [21–24]. Field observations and model simulations indicate four potential sources of dFe to the Ross Sea surface waters: Circumpolar Deep Water (CDW) intruding from the shelf edge, sediments on shallow banks and nearshore areas, melting sea ice around the perimeter of the polynya and glacial meltwater from the Ross Ice Shelf (RIS) [25]. Fe availability and its influence on phytoplankton structure and nutrient cycling has been extensively studied in the Ross Sea [26–31]. Fe limitation has been reported in offshore waters north of the continental shelf, but evidence suggests that Fe limitation is important in the highly productive shelf area too [32–34]. Our understanding of the distribution and speciation of dFe in the Ross Sea has been improved significantly in the past two decades; however, there have only been a few studies on their mesoscale variability. To fill this lack, the Ross Sea Mesoscale Experiment (RoME) was designed to investigate the short temporal and small spatial scales (i.e. mesoscale with an horizontal resolution of few km) variability of biogeochemical properties of the upper 200 m layers in the Ross Sea and to study their interaction with mesoscale currents, fronts and eddies that can facilitate the supply of dFe to the surface waters.

RoME used a combination of remote sensing and high-resolution ship measurements during a cruise in the austral summer 2013–14, as a part of the Italian National Program of Research in Antarctica (PNRA, Programma Nazionale di Ricerca in Antartide). Remote sensing supported both the determination of the iron sampling strategy and the deployment of 43 complete casts, with a horizontal resolution of 5–10 km. Near-real-time satellite images of the study area were sent twice a day to the research vessel in order to design the sampling strategy. The sampling activity was performed in three different areas of the Ross Sea, named RoME 1, 2 and 3. The aim of the present paper is to characterise the mesoscale iron speciation in the RoME 2 site, a coastal area next to the recurrent winter Terra Nova Bay polynya. This polynya plays a major role in shaping the sea ice and ocean dynamics of this region [35,36] and is characterised by high biological primary production which favours atmospheric carbon sequestration into the ocean [38]. Additionally, previous papers showed the presence of significant chemical and biological mesoscale variability in the RoME 2 area, mainly connected to the different water mass properties observed and to the presence of a thermohaline front associated to changes in the current pattern [11,37,38].

## 2. Materials and methods

### 2.1. Sampling strategy and water sampling

The data were collected aboard the R.V. *Italica*, as part of RoME 2 area from 26 to 28 January 2014. The RoME 2 study area has an extension of ca.  $35 \times 30$  km and was monitored through 12 complete multi-parameter casts. The position of the CTD stations (Figure 1) was chosen on the basis of the available MODIS (Moderate Resolution Imaging Spectroradiometer) Aqua and Terra satellites level-2 products relative to the previous 12/24 hours. Sea surface temperature (SST) and chlorophyll-a concentration (Chl-a) maps at 1 km resolution were generated, analysed and transmitted to the ship to allow sampling of both high and low chlorophyll and temperature regions. Full depth hydrographic casts, current measurement and water sampling were carried out using a SBE 9/11 Plus CTD, with dual temperature and conductivity sensors, coupled with a SBE 32 plastic coated carousel sampler, on which twenty-four 12-L Niskin bottles and a couple of Acoustic Doppler Current Profiler (ADCP) were mounted. The properties of the ocean deep layers will not be treated in this paper, because the objectives of the RoME Project were focused on the upper 200 m of the water column.

During RoME 2, a total of 12 casts was realised and in each cast, 5–7 depths (2–200 m, chosen according to the fluorescence profiles) were sampled for dissolved oxygen, nutrients, phytoplankton pigments and total prokaryote biomass determination. At selected stations (Figure 1 and Table 1), seawater samples for iron analysis were collected by a 20-L teflon-lined GO-FLO bottle (General Oceanics Inc.) which was deployed on a kevlar 6 mm diameter line and closed using a PVC messenger. Seawater was transferred in acid-cleaned (see Section 2.2.1) 2-L low-density polyethylene (LDPE) bottles and immediately treated as reported below (see Section 2.2.2).

### 2.2. Analytical procedures

#### 2.2.1. Cleaning procedures for iron analysis

All the materials coming into contact with the samples were extensively acid-cleaned and the final cleaning conditions were checked by inductively coupled plasma mass spectrometry (ICP-MS). In particular, 2-L LDPE bottles for seawater collection (Nalgene, Rochester, NY, USA) and the polycarbonate (PC) filtration apparatus (Sartorius, Goettingen, Germany) were cleaned as follows: (1) 1% (v/v) tracepur® HNO<sub>3</sub> (Merck, Darmstadt, Germany) for 2–3 days; (2) rinsing 3 times with ultrapure water (Milli-Q from Merck-Millipore); (3) 0.1% (v/v) suprapur® HNO<sub>3</sub> (Merck) for 2–3 days; (4) rinsing 3 times with ultrapure water. The 0.4- $\mu$ m PC filters membranes (HTTP04700 Isopore™ by Millipore) and the 200-mL polypropylene (PP) bottles (VWR International, Radnor, PA, USA) used for the collection and storage of filtered samples were cleaned with the same procedure, but using two-times lower acid concentration and suprapur® grade quality acid for both steps (1) and (3). PC 85-mL centrifuge tubes (Nalgene) for the co-precipitation procedure (Section 2.2.2) were acid-cleaned following the five-step procedure reported in [45]. PP 50-mL and 15-mL graduated tubes (VWR International) for iron speciation analysis were cleaned using 0.1% (v/v) HNO<sub>3</sub> (TraceSelect® Ultra from Sigma-Aldrich) and thoroughly rinsed with ultrapure water.

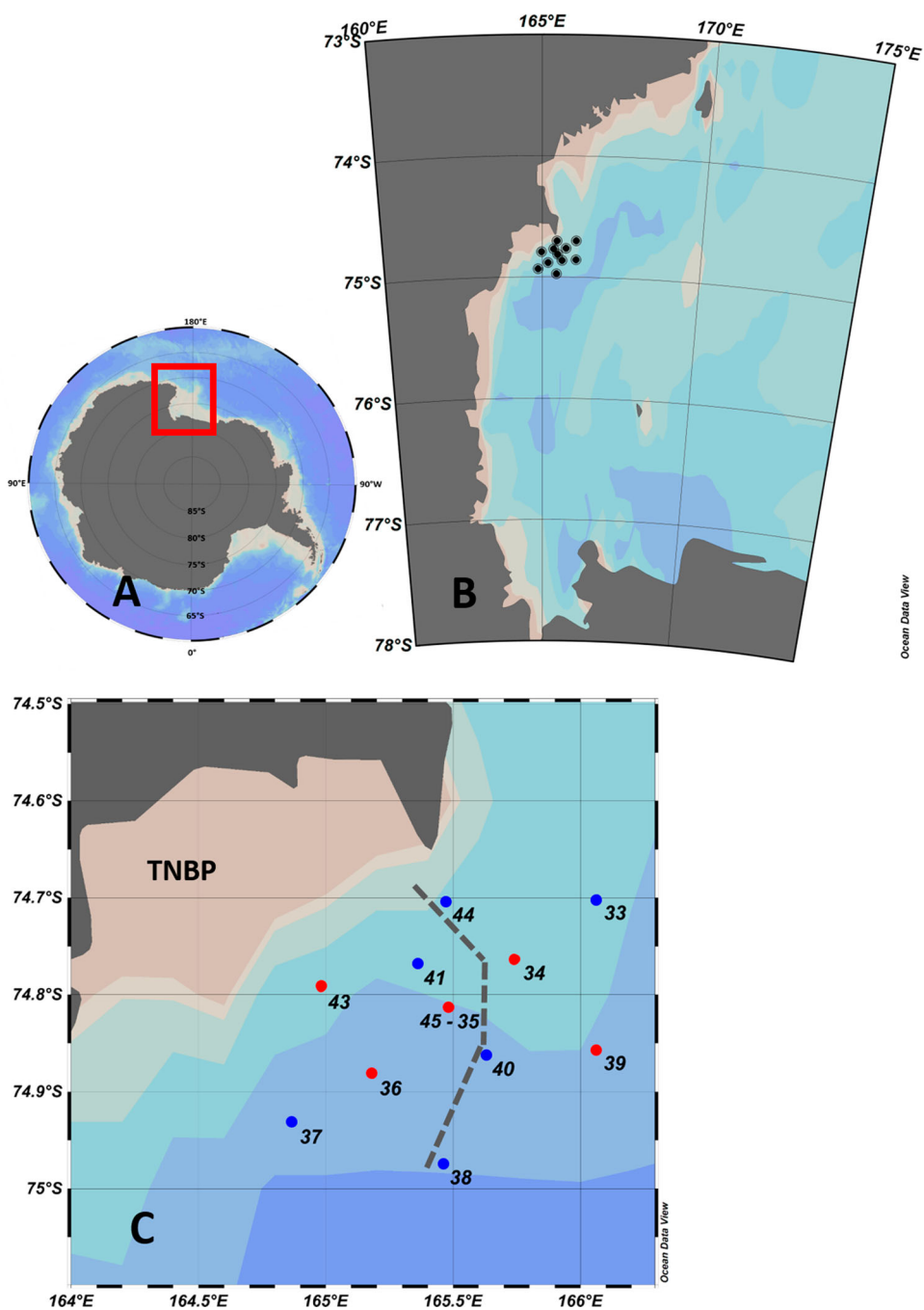


**Figure 1.** Map of the study site RoME 2 in the Ross Sea. (A) the Ross Sea inside the Southern Ocean; (B) the sampled area inside the Ross Sea; (C) the sampled stations: the red dots show the stations sampled for iron and the dashed grey line the position of the front (colour online).

**Table 1.** Sampling stations and collected samples for iron determination.

Station	Latitude (S)	Longitude (E)	Bottom depth (m)	Sampling date	Sampled depths (m)
34	-74.772	165.739	719	26/01/2014	10, 30, 60
36	-74.891	165.193	818	27/01/2014	10, 20, 160
39	-74.860	166.073	1080	27/01/2014	20, 50, 200
43	-74.799	164.990	775	27/01/2014	20, 40, 200
45	-74.826	165.486	702	28/01/2014	10, 25, 200

### 2.2.2. Total dissolved iron

Seawater samples were filtered through 0.4  $\mu\text{m}$  pore-size PC membranes, collected in 200-mL PP bottles and stored at  $-20^\circ\text{C}$  until analysis.

The total dissolved Fe was determined by ICP-MS after a metal pre-concentration procedure through co-precipitation with  $\text{Mg}(\text{OH})_2$  [39], based on a previous work by Wu and Boyle [40]. In brief, under a laminar flow work area, aliquots of seawater samples were acidified (pH 1.8) at least 24 h before analysis. Then, 50.0 g of sample were transferred into an acid-cleaned 85-mL PC centrifuge tube (Nalgene) and 500  $\mu\text{L}$  of concentrated  $\text{NH}_4\text{OH}$  (Trace Select® Ultra from Sigma-Aldrich) were added. After 1.5 min, the tube was quickly shaken and left to stand for 3 min. The sample was centrifuged (3000 rpm, 3 min) and most of the supernatant discarded. Then, the centrifugation was repeated and the remaining solution removed. The resulting precipitate was dissolved in 5 mL of 1% (v/v)  $\text{HNO}_3$  (Trace Select® Ultra from Sigma-Aldrich) and the solution analysed by ICP-MS equipped with a dynamic reaction cell (DRC). The ICP-MS system used was a Perkin Elmer-Sciex (Concord, Ontario, Canada) Elan DRC II, equipped with PFA-ST micronebulizer (Elemental Scientific, Omaha, NE, USA) and a 20-mL inner volume Cinnabar spray chamber (Glass Expansion, Melbourne, Australia). Platinum sampler and skimmer cones were used. The operating conditions (Table 2) were optimised according to Tanner et al. [41]. The monitored ions were  $^{54}\text{Fe}^+$  and  $^{52}\text{Cr}^+$  and the latter was used to correct the isobaric interference due to  $^{54}\text{Cr}^+$  by means of the following equation:  $I(^{54}\text{Fe}) = I(54) - 0.028226 I(^{52}\text{Cr})$ . Since the seawater samples have similar composition, calibration was performed by the 'addition calibration' technique [42], a simplification of the standard

**Table 2.** ICP-MS operating parameters.

Parameter	Value
RF power	1500 W
Plasma gas flow rate	14.5 $\text{L min}^{-1}$
Auxiliary gas flow rate	1.65 $\text{L min}^{-1}$
Nebulizer gas flow rate	1.00 $\text{L min}^{-1\text{a}}$
Sample uptake rate	100 $\mu\text{L min}^{-1}$
Lens voltage	6 $\text{V}^{\text{a}}$
Reaction cell rod offset	-1 V
Quadrupole rod offset	-8 V
RF amplitude	150 V
Axial field voltage	300 V
Cell path voltage	-28 V
Mathieu stability parameters	$a = 0$ $q = 0.57$
Reaction gas flow rate ( $\text{NH}_3$ )	0.9 $\text{mL min}^{-1}$
Dwell time	100 ms
Sweeps	50
Replicates	10

<sup>a</sup>Optimised daily.

'addition' method, in which the slope obtained for a single representative sample is used for the calibration of the other samples. For each calibration curve, four additions were performed in the 0–6  $\mu\text{g L}^{-1}$  concentration range. The correlation coefficients were higher than 0.999. The procedural blank was  $0.15 \pm 0.06$  nM (mean  $\pm$  SD,  $n = 10$ ), providing a limit of detection ( $3 \times \text{SD}_{\text{blank}}$ ) of 0.18 nM. The accuracy of the analytical method was confirmed by replicated analyses of the seawater reference materials SAFe D1 (found concentration:  $0.81 \pm 0.10$  nM,  $n = 8$ ; consensus concentration:  $\sim 0.65 \pm 0.10$  nM) and SAFe D2 (found concentration:  $0.99 \pm 0.09$  nM,  $n = 12$ ; consensus concentration:  $0.92 \pm 0.03$  nM).

### 2.2.3. Organic complexation of Fe: sample treatment, voltammetric procedure and calculations

Iron speciation was determined by adsorptive cathodic stripping voltammetry (AdCSV) with ligand competition against 2,3-dihydroxynaphtalene (DHN) [43,44].

Under a laminar flow work area, the samples were thawed at ambient temperature and homogenised before transferring 50-mL aliquots into 50-mL PP graduated tubes (VWR International). Then, 250  $\mu\text{L}$  of 0.1 mM methanolic solution of DHN (Sigma-Aldrich) were added and the samples were mixed to obtain a final concentration of 0.5  $\mu\text{M}$  DHN. Incremental additions of Fe(III) standard solution were added to eight 15-mL PP graduated tubes and a 6-mL aliquot of the sample/ligand solution prepared above was pipetted into each tube. The concentrations of Fe(III) additions were selected according to the total Fe concentration of each sample, with approximately four increments in the competition region and four increments where the ligands are saturated. The samples were then left to equilibrate overnight (15 h) in the dark (to prevent the slow oxidation of DHN).

Voltammetric measurements were performed using the 757 VA Computrace system by Metrohm (Herisau, Switzerland), equipped with a mercury drop electrode, Ag/AgCl reference electrode and glassy carbon counter-electrode. The working electrode was filled with 99.999% mercury (Sigma-Aldrich), and the 3M KCl (Sigma-Aldrich) filling solution of the reference electrode was cleaned by  $\text{MnO}_2$  co-precipitation [43]. The equilibrated solutions were sequentially (starting from the lowest concentration) transferred into the Teflon<sup>®</sup> voltammetric cell; then, after addition of 300  $\mu\text{L}$  of bromate/3-[4-(2-hydroxyethyl)-1-piperazinyl]propanesulfonic acid (HEPPS) buffer/oxidant solution (0.4 M potassium bromate/0.1 M HEPPS/0.05 M ammonium hydroxide, all from Sigma-Aldrich) to obtain a pH of 8.0, they were analysed by AdCSV, according to the following method [43]:  $\text{N}_2$  purge for 300 s; adsorption potential:  $-0.1$  V; adsorption time: 90 s; rotating speed: 2400 rpm; equilibration time: 8 s; voltage scan: from  $-0.3$  to  $-0.8$  V; scan type: sampled-DC (potential step: 4 mV; frequency: 10 Hz). Four replicate measurements were performed for each aliquot. The voltammetric cell was not rinsed during the titration to keep the cell conditioned. After each sample was analysed, the cell was soaked overnight in 0.5% (v/v)  $\text{HNO}_3$  and then thoroughly rinsed with ultrapure water and pre-conditioned before use.

Calculation of the iron speciation parameters was performed by using the following equation [45,46]:

$$\frac{[\text{Fe}_{\text{labile}}]}{[\text{FeL}]} = \frac{[\text{Fe}_{\text{labile}}]}{L} + \frac{\alpha'_{\text{Fe}} + \alpha'_{\text{FeDHN}}}{L \cdot K'_{\text{FeL}}} \quad (1)$$

where  $[Fe_{labile}]$  (labile Fe) in each aliquot was computed by the ratio of the measured peak height to the instrumental sensitivity, while  $[FeL]$  (organically bound Fe) was obtained as the difference between the total Fe concentration and labile Fe. The sensitivity was iteratively calculated according to Turoczy and Sherwood [47], and the obtained values were in good agreement (within 10%) with those computed by using the non-linear fitting model by Gerringa et al. [48].

A plot of  $[Fe_{labile}]/[FeL]$  as a function of  $[Fe_{labile}]$  allowed the determination of  $L$  (ligand concentration) and  $K'_{FeL}$  (conditional stability constant, here expressed with respect to  $Fe^{3+}$ ), which were used to calculate the side reaction coefficient of  $Fe^{3+}$  and the ligands ( $\alpha'_{FeL}$ ). The side reaction coefficient for inorganic complexation  $\alpha'_{Fe} = 10^{10}$  was obtained from Hudson et al. [49], while  $\alpha'_{FeDHN} = 6.4 \times 10^{12}$  was calculated by Laglera et al. [44] and used also to calculate the  $Fe'$ , i.e. Fe not bound to organic ligands. Finally,  $L'$  (concentration of ligands not bound to Fe) was computed as a difference between  $L$  and  $dFe$  [50].

The method is characterised by great sensitivity, low limits of detection and short analysis time [43]. On the other hand, as other procedures, it is susceptible to potential interferences by humic substances, which would result in an underestimation of the complexing capacity of the natural ligands, as highlighted by a loss of the curvature of the titration plot [44]. A previous investigation in the same area and season reported concentrations of fulvic acids lower than  $0.2 \text{ mg L}^{-1}$ , while humic acids were not found [51]. In addition, curved titration plots were always obtained (e.g. Figure 2), suggesting a negligible interference of these substances, although humic complexation cannot be completely ruled out.

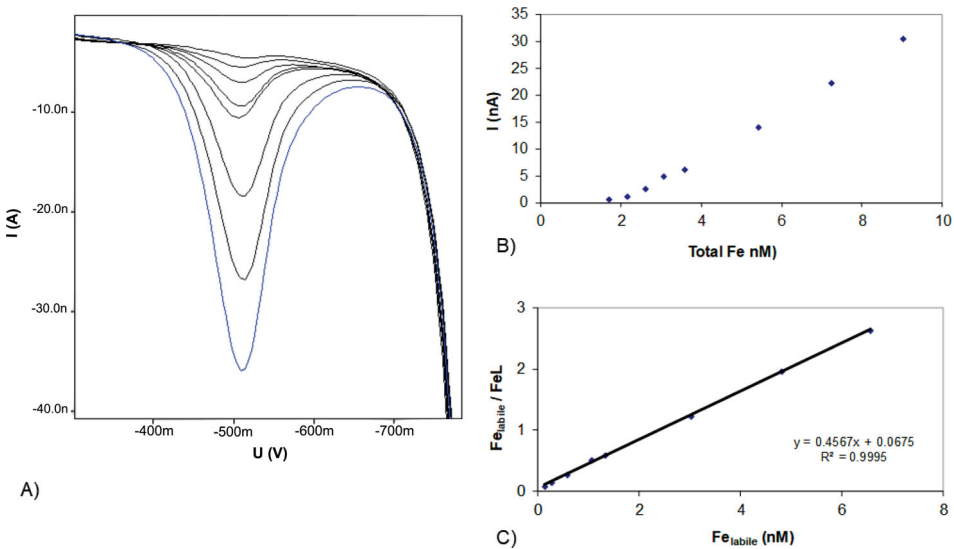


**Figure 2.** Speciation analysis of seawater sampled in Station 55 at 60 m. (A) Voltammetric scans for the titration with iron; (B) peak height as a function of the total iron concentration; (C) data linearisation with  $Fe_{labile}/FeL$  as a function of  $Fe_{labile}$ .



### 2.2.4. Dissolved oxygen, nutrients, phytoplankton pigments and total prokaryote biomass

Dissolved oxygen ( $O_2$ ) was measured by the Winkler method using automated micro-titrations [52] with a potentiometric detection of the end point using a Metrohm 719 titroprocessor. The measurement precision was  $\pm 0.05 \text{ mg L}^{-1}$ .

Subsamples for the determination of nutrients ( $\text{NO}_3^-$ ,  $\text{NO}_2^-$ ,  $\text{NH}_4^+$ ,  $\text{Si(OH)}_4$  and  $\text{PO}_4^{3-}$ ) were collected from the Niskin bottles, filtered through  $0.7 \mu\text{m}$  glass fibre filters (GFF) and stored at  $-20^\circ\text{C}$  in 100 mL LDPE containers. The samples were analysed using a five-channel continuous flow Technicon® Autoanalyzer II, according to the method described by Hansen and Grasshoff [53], which was adapted to our instrumentation. The accuracy and the precision of the method were checked by Certified Reference Material (CRM) MOOS-3 (Seawater Certified Reference Material for Nutrients; [http://www.nrc-cnrc.gc.ca/eng/solutions/advisory/crm/certificates/moos\\_3.html](http://www.nrc-cnrc.gc.ca/eng/solutions/advisory/crm/certificates/moos_3.html)). Measurement precision was  $0.3 \mu\text{M}$  for  $\text{NO}_3^- + \text{NO}_2^-$ ,  $0.01 \mu\text{M}$  for  $\text{NO}_2^-$ ,  $0.07 \mu\text{M}$  for  $\text{PO}_4^{3-}$  and  $0.30 \mu\text{M}$  for  $\text{Si(OH)}_4$ . The recoveries fell in the 100–110% range.

Subsamples for the determination of phytoplankton biomass, taxonomic composition and  $F_v/F_m$  were collected in the 0–100 m depth layer. For a more detailed description of the methods and of the data see Mangoni et al. [11] and Rivaro et al. [37].

For total prokaryote abundances, samples of 50 mL of seawater were collected directly from the Niskin bottles and fixed with a formaldehyde solution (pre-filtered through a  $0.2 \mu\text{m}$  Acrodisc filter) at 2% final concentration. Aliquots of 3–5 mL were filtered in triplicate onto  $0.2 \mu\text{m}$  black polycarbonate membranes (Whatman). The membranes were then placed on a drop (50  $\mu\text{L}$ ) of DAPI (4,6-diamidino-2-phenyl-indole, Sigma-Aldrich,  $30 \mu\text{g mL}^{-1}$  final concentration in an autoclaved 3.7% NaCl solution) and kept in the dark for 15 min [54]. The backs of the filters were then gently dried with a kimwipe tissue, mounted on microscope slides between layers of immersion oil (type A, Cargille) and stored at  $-20^\circ\text{C}$ . Cells were counted by epifluorescence microscopy (Olympus BX 60 F5) at  $1000\times$  magnification under a UV (BP 330–385 nm, BA 420 nm) filter set. A minimum of 300 cells was counted for each membrane in at least 20 randomly selected fields. Prokaryotic biomass was calculated by adopting the  $20 \text{ fg C cell}^{-1}$  factor [55].

### 2.3. Ancillary data and data processing

Meltwater percentage in the surface layer (MW%) was calculated from the difference between the salinity measured at the surface ( $S_{\text{meas}}$ ) and at greater depth ( $S_{\text{deap}}$ , i.e. 200 m) and assuming an average sea ice salinity of 6 [34]:

$$\text{MW}\% = 1 - \frac{S_{\text{meas}} - 6}{S_{\text{deap}} - 6} \cdot 100 \quad (2)$$

All the available CTD profiles were used to determine the depth of the Upper Mixed Layer (UML) through the water column stability (E) analysis. E is proportional to the Brunt-Väisälä buoyancy frequency  $N^2(z)$ , which represents the strength of the density stratification. The depth at which  $N^2(z)$  was estimated to be maximal represents the depth of maximum stability and was selected to represent the UML depth  $z(\text{UML})$  [56].

Data processing and statistical analysis were performed using the software RStudio version 0.97.318 (RStudio Inc., Boston, MA, USA). Relationships between all parameters

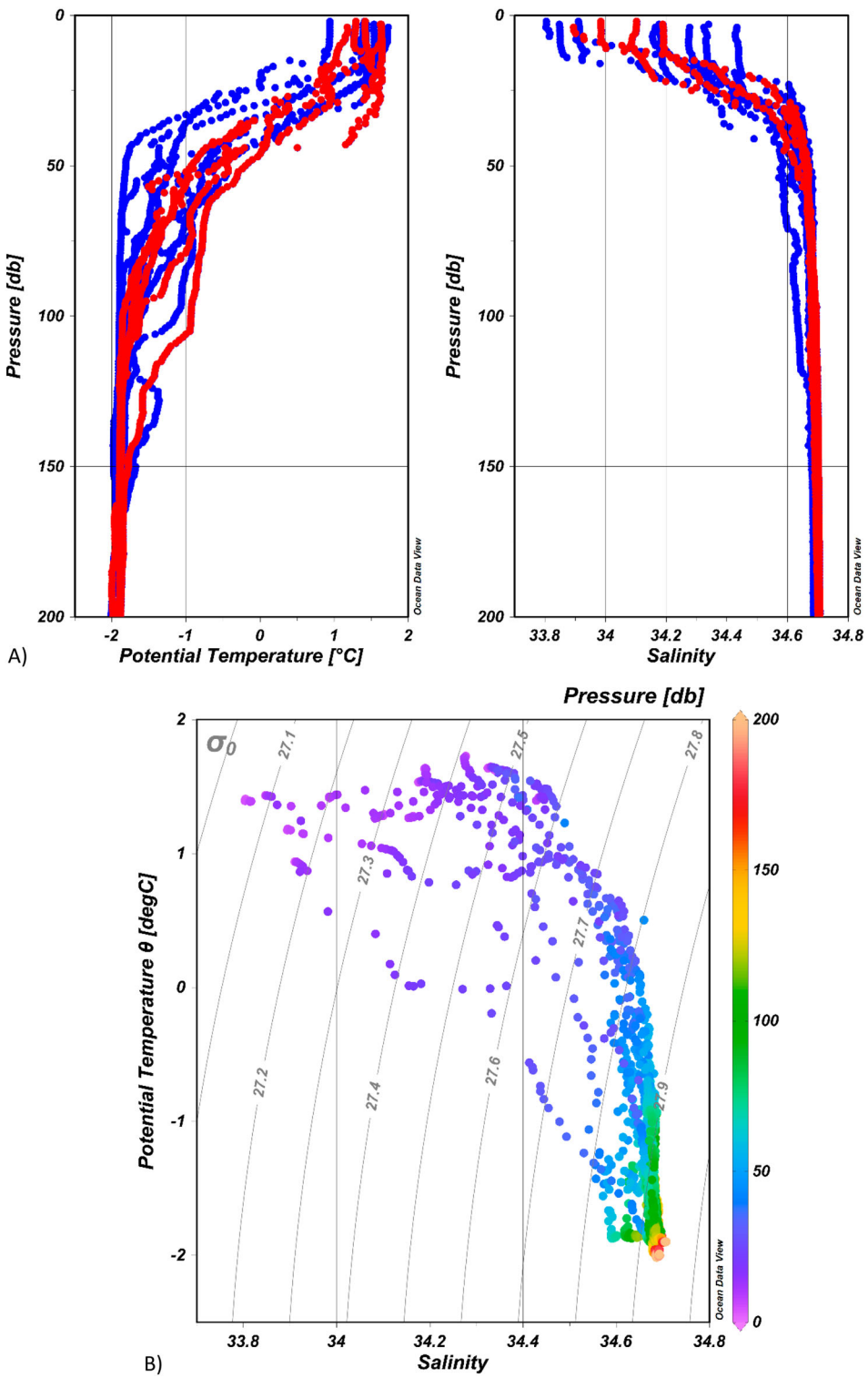
were evaluated by means of the Pearson's correlation coefficient ( $r$ ) and the Spearman coefficient ( $\rho$ ) of rank correlation, after assessing normality of datasets to choose between parametric and non-parametric statistics. The maps were drawn with Ocean Data View software [57].

### 3. Results

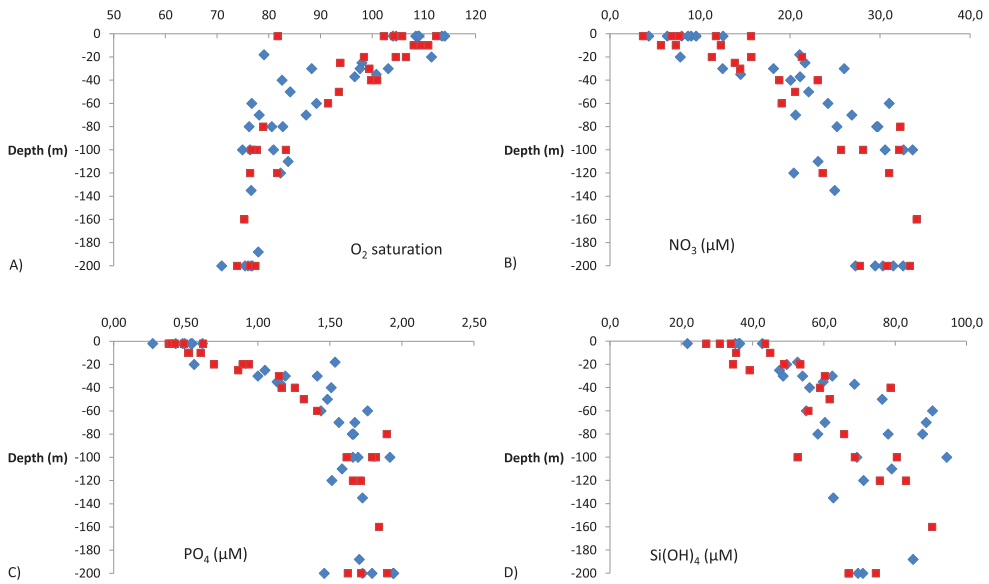
#### 3.1. Environmental conditions and biogeochemical properties

Figure 3 shows the main hydrographic features observed during the RoME 2 experiment. Properties of the water masses and the circulation patterns of the three RoME legs have been already reported and discussed in Mangoni et al. [11], Rivaro et al. [37] and Misić et al. [38]. In RoME 2, the surface (0–100 m depth) and intermediate layers (100–200 m depth) of the water column were mainly occupied by Antarctic Surface Water (AASW) and High Salinity Shelf Water (HSSW) respectively (Figure 3). AASW is a relatively light surface water characterised by potential temperatures ranging between  $-1.8^{\circ}\text{C}$  and  $+1^{\circ}\text{C}$  and by salinity values lower than 34.50, while HSSW is characterised by salinity greater than 34.70, potential temperature near freezing point and potential density greater than  $27.9 \text{ kg m}^{-3}$  [58]. The mean circulation during the RoME 2 experiment was characterised by the presence of a meridionally oriented frontal zone located at about  $165.5^{\circ}\text{E}$ . This front (grey dashed line in Figure 1) has been extensively described in [37] and represents the boundary between two circulation systems characterised by different thermohaline properties and current regime (see Figure 3 and 7 in [37]). In particular, colder and fresher water masses are observed on the western flank of the front and their eastward extension is limited by the front itself. Crossing the front, an increase in both temperature and salinity of the surface layer is evident, with stations located in proximity of the front showing intermediate T and S values between the coastal and open sea stations. Current pattern as depicted by both LADCP and geostrophic current data (not shown) is characterised by eastward current in the coastal stations and prevalently southward currents on the eastern side of the front generating a convergence in correspondence of the front [37].

The water column was well stratified all over the study area, but differences in UML depth and in the strength of the pycnocline were observed [11]. Almost all stations were above the  $\text{O}_2$  saturation level (102–115%) in the upper 20 m (Figure 4, panel A). Nutrient concentrations were generally high, with the lowest values in surface and subsurface layers and they were not fully depleted (Figure 4, panels B, C and D). The N:P ratio (calculated from the slope of  $\text{NO}_3^- + \text{NO}_2^-$  plotted against  $\text{PO}_4^{3-}$ ) of 17.0 was consistent with the phytoplankton taxonomic composition data that highlighted the concurrence of diatoms and *P. antarctica* [11,37]. The Si:NO<sub>3</sub> ratio was about 1 suggesting Fe-replete condition, as proven by the dFe data, similarly to previous investigations in the Ross Sea shelf and coastal areas [17,27,28,34]. The net nutrient utilisation was estimated by subtracting the nutrient concentration measured in the UML from that measured in the Winter Water (WW) layer, assuming that the nutrient values in surface water at the beginning of the growing season are similar to those in WW, which are not affected by meltwater dilution or biological uptake [59]. In this study, the concentration of nutrients measured at the depth below the UML, at the top of the WW layer depth  $z(L)$ , is considered as the reference value for WW (Table 3).



**Figure 3.** (A) Potential temperature (ITS-90) and salinity (practical) profiles of RoME 2 stations. Red dots show the stations sampled for iron. (B)  $\theta/S$  diagram colour coded with depth (colour online).



**Figure 4.** Depth profiles of: (A) dissolved oxygen saturation percentage; (B) nitrate; (C) phosphate and (D) silicate area. Squares show the stations sampled for iron, diamonds refer to the other sampled stations.

The calculated net nutrient utilisation ranges for nitrate, silicic acid and phosphate ( $\Delta\text{NO}_3^-$ ,  $\Delta\text{Si(OH)}_4$  and  $\Delta\text{PO}_4^{3-}$ ) were 4.6–13.6, 3.6–24.1 and 0.26–0.82  $\mu\text{M}$ , respectively (Table 3). The highest  $\Delta\text{NO}_3^-$ , which corresponds to the highest  $\Delta\text{PO}_4^{3-}$ , was measured in station 43. The net nutrient utilisation values were in the range of the reported values for the Ross Sea shelf area [59].

Prokaryotic biomass values in the upper 70 m did not display any depth-related trend and ranged between 11.30 ( $\pm 0.45$ ) and 14.41 ( $\pm 1.06$ )  $\mu\text{g C L}^{-1}$ . Lower values were found between 160 and 200 m, being on average  $1.31 \pm 0.17 \mu\text{g C L}^{-1}$ . A highly significant correlation with Chl-a (Spearman's  $\rho = 0.65$ ;  $p < .001$ ;  $n = 32$ ) was found.

Data on phytoplankton biomass, taxonomic composition and  $F_v/F_m$  collected in the framework of the RoME project have been already published [11,37,38]. As concerns RoME 2 area, Chl-a maxima were measured from 20 to 40 m depth, but high Chl-a values were also found at greater depth in some stations (up to 2.48  $\mu\text{g L}^{-1}$  at 100 m at station 45). Diatoms, which were observed with empty frustules and in a senescent status, constituted the dominance of the phytoplankton in the upper layer, whereas *Phaeocystis antarctica* in the colonial form dominated in the deep layers. With regards to the photochemical efficiency of

**Table 3.** Values of strength (Ez(UML)) and depth of the maximum stability (z(UML)) of the upper mixed layer, top of the Winter Water depth (z(L)), meltwater percentage (MW%) and calculated nutrient removal ( $\Delta\text{NO}_3^-$ ,  $\Delta\text{Si(OH)}_4$ ,  $\Delta\text{PO}_4^{3-}$ ).

Station	Ez(UML) ( $\text{m}^{-1} * 1000$ )	z(UML) (m)	z(L) (m)	MW (%)	$\Delta\text{NO}_3^-$ ( $\mu\text{M}$ )	$\Delta\text{PO}_4^{3-}$ ( $\mu\text{M}$ )	$\Delta\text{Si(OH)}_4$ ( $\mu\text{M}$ )
34	55	32	66	2.09	6.93	0.49	3.57
36	59	16	54	2.51	5.46	0.47	19.3
39	87	25	71	1.23	6.73	0.50	7.59
43	44	26	75	2.83	13.4	0.82	16.8
45	40	18	60	1.80	6.14	0.48	12.1

photosystem II of phytoplankton, the values of  $F_v/F_m$  were lower in the presence of diatoms-dominated waters compared with *P. antarctica*-dominated waters.

### 3.2. Total dissolved iron and iron speciation

Total dissolved iron (dFe) and speciation data are presented in Table 4. The dFe concentration ranged from 0.52 to 4.51 nM, L from 1.4 to 8.0 nM and Fe' from 0.2 to 3.5 pM. The dFe concentrations are comparable with values reported for Antarctic coastal waters [29,34,60–63], and significantly higher than those found in open waters [26]. More than 99% of dFe in our samples was bound to organic ligands, similarly to other seawater analysis carried out in the Southern Ocean [64]. The L values exceeded dFe in all the samples and, as a consequence, L' varied from 0.12 to 2.11 nM. A significant positive correlation was observed between L and dFe (Spearman's  $\rho = 0.96$ ,  $p < .001$ ,  $n = 13$ ). The L/dFe ratio is used to evaluate the saturation level of dissolved organic ligands in the marine environment [65]. When it is close to 1 the ligands are relatively saturated, whereas a higher ratio suggests that the ligands are still available to buffer additional Fe input. The L/dFe varied between 1.07 and 2.82; similar values have been already reported by Boye et al. [17] for Southern Ocean and by Thuróczy et al. [65] for Amundsen Sea shelf waters.

The conditional stability constant ( $\log K'_{FeL}$ ) varied over one order of magnitude, ranging from 22.1 to 23.6; these values are consistent with those reported for the strongest ligands found in the Southern Ocean [48,64,66].

The side reaction coefficient of iron complexation by the natural ligands ( $\log \alpha'_{FeL}$ ) ranged between 13.3 and 14.6, with an average of  $14.0 \pm 0.5$  ( $n = 13$ ).

## 4. Discussion

The water column properties in the Ross Sea exhibit high levels of spatial and temporal variability and seem to be also linked to larger scales patterns [5,67]. Unfortunately, due to the difficulty in obtaining high-frequency observations, the effect of the mesoscale physical processes on biological and chemical distributions is poorly known, but is still likely to be significant [67]. For this reason, the sampling strategy of the RoME cruise was designed on the basis of real-time satellite data, with the aim of examining selected

**Table 4.** Iron speciation data.

Station	Depth (m)	dFe (nM)	L (nM)	SD	$\log K'_{FeL}$	SD	L' (nM)	L/dFe	Fe' (pM)	FeL (%)	$\log \alpha'_{FeL}$
34	10	2.10	4.2	0.1	22.5	0.2	2.11	2.00	0.3	100.0	14.1
	30	1.19	1.7	0.1	22.5	0.1	0.48	1.41	0.8	99.9	13.7
	60	1.95	2.8	0.1	22.8	0.1	0.83	1.43	0.4	100.0	14.2
36	10	0.57	1.4	0.1	22.3	0.1	0.81	2.42	0.3	99.9	13.5
	160	1.80	1.9	0.1	23.3	0.4	0.12	1.07	0.7	100.0	14.6
39	20	1.80	2.5	0.1	22.7	0.1	0.73	1.41	0.5	100.0	14.1
	50	1.21	1.9	0.1	22.7	0.1	0.65	1.54	0.4	100.0	13.9
	200	4.51	5.0	0.1	22.8	0.1	0.48	1.11	1.5	100.0	14.5
43	20	0.65	1.8	0.1	22.2	0.1	1.18	2.82	0.4	99.9	13.4
	40	0.52	1.5	0.1	22.1	0.1	0.99	2.91	0.4	99.9	13.3
	200	3.19	5.0	0.1	22.6	0.1	1.76	1.55	0.4	100.0	14.3
45	10	1.97	–	–	–	–	–	–	–	–	–
	25	1.82	2.0	0.1	23.6	0.6	0.19	1.10	0.2	100.0	14.9
	200	3.29	3.7	0.1	22.3	0.1	0.44	1.13	3.5	99.9	13.9

mesoscale features in detail and to study the biogeochemical processes associated to them. In this framework, the spatial coverage of the RoME 2 area was of ca.  $35 \times 30$  km and was monitored through 12 complete multi-parameter casts and a set of near real-time satellite images.

A thermohaline front was the main physical feature of the area (cf. Figure 1), with the surface layer characterised by a temperature and salinity gradient between the coastal and the easternmost and open ocean station. Fresh and cold water, possibly influenced by both sea or glacier ice melting and then driven offshore by eastwards currents, was observed at stations 41, 43, 44 sampled near Cape Washington and inner bay [11,37,38].

The higher dFe concentration found in the RoME 2 area in the subsurface waters compared with offshore waters (Figure 5, panel G) reflects the iron input either from land [29] or from ice melting, similar to the observations made by Sedwick et al. [28] at stations sampled at the edge of the receding annual pack ice. The iron cycle is closely related to the dynamics of sea ice that acts as a reservoir for iron during winter, releasing it to the surface ocean in spring and summer [68]. The area experienced ice-free conditions starting from early December [11,37]. The melting produced a strong water column stratification highly favourable for iron recycling, through the enrichment of Fe for surface waters and retarding the loss of Fe to deeper waters. Dissolved Fe concentrations were relatively low near the surface in correspondence of the highest MW% (Figure 5, panel C, stations 36 and 43). This apparent contradiction can be explained taking into account the role of the UML stratification in favouring the phytoplankton growth (Figure 5, panels A, B and D). In fact, a reduction in the dFe may be associated with an increase in algal biomass as the iron is taken up. The melting of the sea ice, besides stratifying the water column, supported the phytoplankton growth, as the negative correlation found between dFe and fluorescence (Spearman's  $\rho = -0.60$ ,  $p < .05$ ,  $n = 14$ ) together with the  $O_2$  values above the saturation level, the nutrient utilisation and the Chl-a concentrations confirmed (Figure 5, panels E

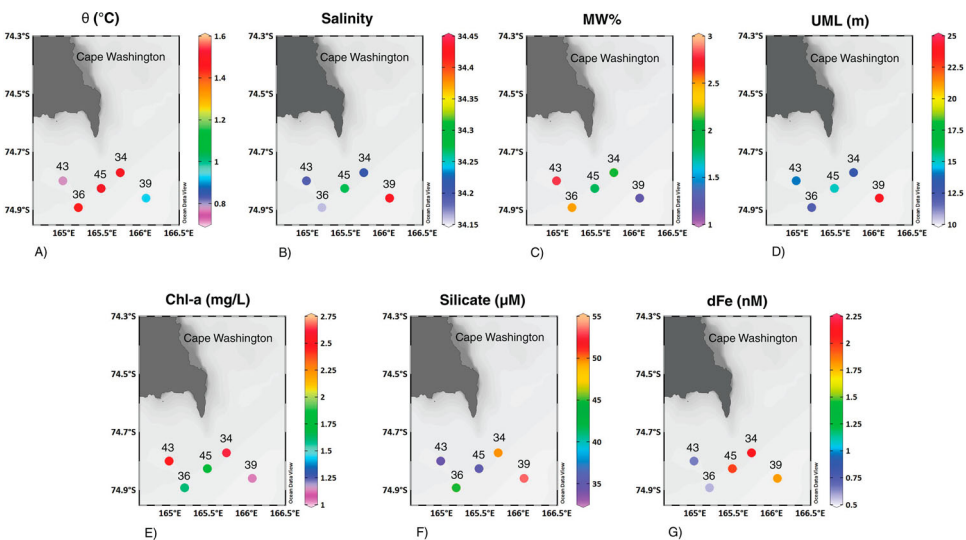


**Figure 5.** Subsurface distribution of: (A) potential temperature ( $\theta$ ); (B) salinity; (C) meltwater percentage (MW%); (D) upper mixed layer (UML) depth; (E) chlorophyll-a (Chl-a); (F) silicate ( $Si(OH)_4$ ); (G) total dissolved iron (dFe).

and F). Changes in PS II efficiency are assumed to reflect the 'photosynthetic health' of the phytoplankton and to be affected mainly by cellular acclimations to changing abiotic conditions (including nutrient availability, especially N and Fe) [10,69]. However, from the Si: NO<sub>3</sub> ratio in the upper layer, that suggested Fe-replete condition, we conclude that the reduced  $F_v/F_m$  detected at the surface was not due to Fe limitation. The correlation between dFe and L (Spearman's  $\rho = 0.96$ ,  $p < .001$ ,  $n = 13$ ) demonstrated that organic ligands maintained the concentrations of dFe at levels much higher than the inorganic solubility of Fe, keeping it available for phytoplankton [14]. Ligand distribution did not co-vary with Chl-a, but it negatively and significantly co-varied with prokaryotic biomass (Pearson's  $r = -0.62$ ,  $p < .05$ ,  $n = 11$ ) suggesting a role of microbial activities in determining L distribution. However, it should be noted that the variations in ligand concentrations in the surface layer are the result of a balance between production and breakdown processes, including photo-chemical reactions, which can obscure a possible relationship between L and the biomass parameters [70,71]. In oceanic waters, iron-complexing ligands comprise a wide range of organic species, including humic substances, siderophores and biological degradation/extraction products (e.g. exopolymeric substances and saccharides), characterised by different production and loss pathways, functions and reactivity [14]. According to their binding affinities for iron, the ligands can be divided into different classes: L<sub>1</sub> includes stronger ligands, with  $\log K'_{FeL} = 22-23$  or higher, while L<sub>2</sub>- to L<sub>4</sub>- types gather weaker ligands, with  $\log K'_{FeL} = 20-22$  or lower [64]. Siderophores usually fall in the first group, although a photoactive siderophore belonging to the L<sub>2</sub> class has been reported, while exopolymeric and humic substances belong to the L<sub>1</sub>-L<sub>2</sub> and L<sub>2</sub>-L<sub>3</sub> classes, respectively. Finally, saccharides have a weak affinity for iron (L<sub>3</sub>-L<sub>4</sub> classes), but can compete with the L<sub>1</sub> class for iron binding when occurring at a relatively high concentration [72]. The  $\log K'_{FeL}$  values found in the RoME 2 area (22.1-23.6) highlighted the presence of complexes of differing stabilities, which could not be differentiated with the applied method, thus masking possible trends with depth, or distance, from shore [14,17]. The published data for the Southern Ocean, in which L<sub>1</sub> and L<sub>2</sub> ligands could be distinguished [64,66], reported  $\log K'_{L1} = 22.3-23.6$  and  $\log K'_{L2} = 21-22$ . Therefore, our data would indicate the presence of L<sub>1</sub>-type ligands. On the other hand, the values found in the surface waters of the fresher coastal stations 36 and 43 (22.2-22.3) are also consistent with data obtained for the iron complexes in under-ice seawater (21.2-22.1), attributed to exopolymeric substances [73]. Below the UML (where  $\log K'_{FeL}$  values ranged from 22.1 to 23.3), *P. antarctica* was observed in a colonial form and in good physiological status [11]. The mucilaginous matrix that encapsulates the cells is composed of polysaccharides, with a high carbohydrate content, embedding floating of particulate organic matter and dissolved organic matter [74]. We can speculate that the mucilage, besides providing ecological niches for microbial heterotrophs [75], can play the role as a Fe binding ligand, although their Fe binding strength is relatively lower than what we found. Therefore, in this way, it could sustain the bloom of *P. antarctica*.

## 5. Conclusions

The distribution of dFe and iron speciation in the upper 200 m layers of the water column was investigated in a coastal area of the Ross Sea during the austral summer 2014. Our results document substantial spatial heterogeneity and complexity in iron distribution

and speciation at a horizontal length scale of about 10 km, emphasising the importance of mesoscale physical events, such as front, to regional biogeochemistry. Nutrients and iron were above any limiting growth concentration reported for the Ross Sea during summer. The high dFe concentration is the result of different sources, such as the melting of the sea ice or the delivering from the landmasses. The organic ligands maintained the concentrations of dFe at levels much higher than the inorganic solubility of Fe, keeping it available for phytoplankton. Moreover, the  $\log K'_{\text{FeL}}$  values found highlighted the presence of complexes of differing stabilities, suggesting both autotrophic and heterotrophic contribution to the iron speciation. Further mesoscale measurements of the iron speciation in the Ross Sea will provide insights into the iron sources and on the mechanisms controlling the bioavailable species, thus helping the interpretation of data on iron biogeochemical cycle on a large scale. This will be of particular importance considering, for example, the effects of climate change on iron sources (such as the sea ice) and on the physical characteristics of surface waters. For instance, the lengthening of the ice season observed in summer in the Ross Sea, thought to supply iron to surface waters, could induce a considerable increase in phytoplankton biomass which may have a powerful impact on the trophic structure of the entire ecosystem.

## Acknowledgments

The help of the officers and the crew on the R.V. *Italica* is kindly acknowledged. The authors are grateful to Gabriele Capodaglio for providing them with the GO-FLO sampler and to Giuseppe Arena, Federico Angelini and Leonardo Langone for their help during the sampling. The authors thank Elena Soddu for her assistance with the iron measurements, Eugen Behrens and Ivano Vascotto for helping with the prokaryote counts. We are grateful to anonymous referees for their suggestions.

## Disclosure statement

No potential conflict of interest was reported by the authors.

## Funding

This study was conducted in the framework of the project 'Ross Sea Mesoscale Experiment (RoME)' funded by the Italian National Program for Antarctic Research [PNRA, 2013/AN2.04].

## Notes on contributors

**Paola Rivaro** is an associate professor in Chemical Oceanography and Environmental Analytical Chemistry at the Department of Chemistry and Industrial Chemistry in Genoa (Italy). She holds a PhD in Marine Environmental Sciences in Parma-Genoa Universities.

**Francisco Ardini** is a researcher in Analytical Chemistry at the Department of Chemistry and Industrial Chemistry in Genoa (Italy). He earned a PhD in Chemical Sciences and Technologies at the University of Genoa in 2012.

**Marco Grotti** is an associate professor in Analytical Chemistry at the Department of Chemistry and Industrial Chemistry in Genoa (Italy). He holds a PhD in Chemistry at Genoa University.

**Giuseppe Aulicino** received the environmental sciences degree from the University 'Parthenope' in Napoli, Italy, in 2007 and the PhD degree in 'Polar Sciences' from the University of Siena, Siena, Italy, in 2011. Since 2012, he has been a Postdoctoral Research Fellow with the University 'Parthenope' in Napoli and then with the Marche Polytechnic University.



**Yuri Cotroneo** is a researcher at the Department of Science and Technologies (DiST) of the University 'Parthenope' of Naples (Italy), and since 2018 he is a lecturer in Oceanography and Meteorology. He earned a master's degree in 'Environmental Sciences' at University 'Parthenope' of Naples (Italy) in 2003 and then a doctorate in 'Polar Sciences' at the University of Siena (Italy) in 2009.

**Giannetta Fusco** earned the Laurea degree in nautical sciences, major in physical oceanography, in 1996 at the University 'Parthenope' in Napoli, Italy. She is currently with the University 'Parthenope' – Department of Science and Technologies (DiST), where she became an Assistant Professor in 2005 and Lecturer in Polar Oceanography since 2007. From 2008 to 2013 she was Lecturer in Meteorology and Oceanography. From 2013 to present she is Lecturer in Climatology.



**Olga Mangoni** is an associate Professor in Ecology at the 'Federico II' University in Naples (Italy). She earned a science degree in 'Natural Sciences' at the 'Federico II' University in Naples (Italy) and then a PhD in 'Environmental Sciences' at the University of Messina (Italy).

**Francesco Bolinesi** is a PhD student at the Biology Department of University of Naples, Federico II, Naples (Italy), with expertise in Limnology, Marine Biology and Ecology.

**Maria Saggiomo** is a Technologist at the 'Stazione Zoologica Anthon Dhorn' in Naples (Italy). She earned a science degree in 'Natural Sciences' at the 'Federico II' University in Naples (Italy) in 2003 and then a PhD in 'Environmental Sciences' at the University of Messina (Italy) in 2007.

**Mauro Celussi** is a researcher at the Istituto Nazionale di Oceanografia e Geofisica Sperimentale, Trieste, Italy. He holds a PhD in Polar Sciences at the Siena University. He performed research activity in Marine Microbial Ecology.

## ORCID

Paola Rivaro  <http://orcid.org/0000-0001-5412-7371>  
Francisco Ardini  <http://orcid.org/0000-0003-0094-9227>  
Marco Grotti  <http://orcid.org/0000-0001-6956-5761>  
Giuseppe Aulicino  <http://orcid.org/0000-0001-6406-8715>  
Yuri Cotroneo  <http://orcid.org/0000-0002-0099-0142>  
Giannetta Fusco  <http://orcid.org/0000-0003-1769-2456>  
Olga Mangoni  <http://orcid.org/0000-0001-7789-0820>  
Mauro Celussi  <http://orcid.org/0000-0002-5660-6832>

## References

- [1] Morel FMM, Price NM. The biogeochemical cycles of trace metals in the oceans. *Science*. 2003;300:944–947.
- [2] Behrenfeld MJ, Milligan AJ. Photophysiological expressions of iron stress in phytoplankton. *Annu Rev Mar Sci*. 2013;5:217–246.
- [3] Cotroneo Y, Budillon G, Fusco G, et al. Cold core eddies and fronts of the antarctic circumpolar current south of New Zealand from in situ and satellite data. *J Geophys Res Oceans*. 2013;118:2653–2666.
- [4] Buongiorno Nardelli B, Guinehut S, Verbrugge N, et al. Southern Ocean mixed-layer seasonal and interannual variations from combined satellite and In situ data. *J Geophys Res Oceans*. 2017;122:10042–10060.
- [5] Cerrone D, Fusco G, Cotroneo Y, et al. The antarctic circumpolar wave: its presence and inter-decadal changes during the last 142 years. *J Clim*. 2017;30:6371–6389.
- [6] Cerrone D, Fusco G, Simmonds I, et al. Dominant covarying climate signals in the Southern Ocean and antarctic Sea Ice influence during the last three decades. *J Clim*. 2017;30:3055–3072.
- [7] Fusco G, Cotroneo Y, Aulicino G. Different behaviours of the ross and weddell seas surface heat fluxes in the period 1972–2015. *Climate*. 2018;6:17.

- [8] Sosik HM, Olson RJ. Phytoplankton and iron limitation of photosynthetic efficiency in the Southern Ocean during late summer. *Deep Sea Res Part Oceanogr Res Pap.* **2002**;49:1195–1216.
- [9] Arrigo KR, Worthen DL, Robinson DH. A coupled ocean-ecosystem model of the Ross Sea: 2. Iron regulation of phytoplankton taxonomic variability and primary production. *J Geophys Res Oceans.* **2003**;108:3231.
- [10] Hiscock MR, Lance VP, Apprill AM, et al. Photosynthetic maximum quantum yield increases are an essential component of the Southern Ocean phytoplankton response to iron. *Proc Natl Acad Sci USA.* **2008**;105:4775–4780.
- [11] Mangoni O, Saggiomo V, Bolinesi F, et al. Phytoplankton blooms during austral summer in the Ross Sea, Antarctica: Driving factors and trophic implications. *PLOS ONE.* **2017**;12:e0176033.
- [12] Tortell PD, Maldonado MT, Granger J, et al. Marine bacteria and biogeochemical cycling of iron in the oceans. *FEMS Microbiol Ecol.* **1999**;29:1–11.
- [13] Hassler CS, Schoemann V. Bioavailability of organically bound Fe to model phytoplankton of the Southern Ocean. *Biogeosciences.* **2009**;6:2281–2296.
- [14] Gledhill M, Buck KN. The organic complexation of iron in the marine environment: a review. *Front Microbiol.* **2012**;3:69.
- [15] Rue EL, Bruland KW. Complexation of iron(III) by natural organic-ligands in the Central North Pacific as determined by a new competitive ligand equilibration adsorptive cathodic stripping voltammetric method. *Mar Chem.* **1995**;50:117–138.
- [16] Hutchins DA, Witter AE, Butler A, et al. Competition among marine phytoplankton for different chelated iron species. *Nature.* **1999**;400:858–861.
- [17] Boye M, van den Berg CMG, de Jong JTM, et al. Organic complexation of iron in the Southern Ocean. *Deep Sea Res Part Oceanogr Res Pap.* **2001**;48:1477–1497.
- [18] Maldonado MT, Strzepek RF, Sander S, et al. Acquisition of iron bound to strong organic complexes, with different Fe binding groups and photochemical reactivities, by plankton communities in Fe-limited subantarctic waters. *Glob Biogeochem Cycles.* **2005**;19:GB4523.
- [19] Hassler CS, Schoemann V, Boye M, et al. Iron bioavailability in the Southern Ocean. In: Gibson RN, Atkinson RJA, Gordon JDM, et al., editor. *Oceanography and marine biology*. Boca Raton (FL): CRC Press; **2012**. p. 1–64.
- [20] Smith WO, Jr, Ainley DG, Arrigo KR, et al. The oceanography and ecology of the Ross Sea. *Annu Rev Mar Sci.* **2014**;6:469–487.
- [21] Saggiomo V, Carrada GC, Mangoni O, et al. Spatial and temporal variability of size-fractionated biomass and primary production in the Ross Sea (Antarctica) during austral spring and summer. *J Mar Syst.* **1998**;17:115–127.
- [22] Saggiomo V, Catalano G, Mangoni O, et al. Primary production processes in ice-free waters of the Ross Sea (Antarctica) during the austral summer 1996. *Deep Sea Res Part II Top Stud Oceanogr.* **2002**;49:1787–1801.
- [23] Catalano G, Budillon G, La Ferla R, et al. The Ross Sea. In: Liu K-K, Atkinson L, Quiñones R, et al., editors. *Carbon and nutrient fluxes in continental margins: a global synthesis*. Berlin: Springer-Verlag; **2010**. p. 303–318.
- [24] Smith WO, Jr, Dinniman MS, Tozzi S, et al. Phytoplankton photosynthetic pigments in the Ross Sea: patterns and relationships among functional groups. *J Mar Syst.* **2010**;82:177–185.
- [25] McGillicuddy DJ, Sedwick PN, Dinniman MS, et al. Iron supply and demand in an Antarctic shelf ecosystem. *Geophys Res Lett.* **2015**;42:8088–8097.
- [26] Gerringa LJA, Laan P, van Dijken GL, et al. Sources of iron in the Ross Sea Polynya in early summer. *Mar Chem.* **2015**;177:447–459.
- [27] Fitzwater SE, Johnson KS, Gordon RM, et al. Trace metal concentrations in the Ross Sea and their relationship with nutrients and phytoplankton growth. *Deep Sea Res Part II Top Stud Oceanogr.* **2000**;47:3159–3179.
- [28] Sedwick PN, DiTullio GR, Mackey DJ. Iron and manganese in the Ross Sea, Antarctica: seasonal iron limitation in Antarctic shelf waters. *J Geophys Res Oceans.* **2000**;105:11321–11336.
- [29] Grotti M, Soggia F, Abelmoschi ML, et al. Temporal distribution of trace metals in Antarctic coastal waters. *Mar Chem.* **2001**;76:189–209.

- [30] Coale KH, Michael Gordon R, Wang X. The distribution and behavior of dissolved and particulate iron and zinc in the Ross Sea and Antarctic circumpolar current along 170°W. *Deep Sea Res Part Oceanogr Res Pap.* 2005;52:295–318.
- [31] Feng Y, Hare CE, Rose JM, et al. Interactive effects of iron, irradiance and CO<sub>2</sub> on Ross Sea phytoplankton. *Deep Sea Res Part Oceanogr Res Pap.* 2010;57:368–383.
- [32] Coale KH, Wang X, Tanner SJ, et al. Phytoplankton growth and biological response to iron and zinc addition in the Ross Sea and Antarctic Circumpolar Current along 170°W. *Deep Sea Res Part II Top Stud Oceanogr.* 2003;50:635–653.
- [33] Arrigo KR. Physical control of primary productivity in arctic and Antarctic polynyas. In: Smith WOJr, Barber DG, editors. *Polynyas: Windows to the World*. Amsterdam: Elsevier; 2007. p. 223–238.
- [34] Rivaro P, Abemoschi ML, Grotti M, et al. Combined effects of hydrographic structure and iron and copper availability on the phytoplankton growth in Terra Nova Bay Polynya (Ross Sea, Antarctica) *Deep-Sea Res Part Oceanogr Res Pap.* 2012;62:97–110.
- [35] Sansiviero M, Morales Maqueda MÁ, Fusco G, et al. Modelling sea ice formation in the Terra Nova Bay polynya. *J Mar Syst.* 2017;166:4–25.
- [36] Alicino G, Sansiviero M, Paul S, et al. A New approach for monitoring the terra nova Bay polynya through MODIS Ice surface temperature imagery and its validation during 2010 and 2011 winter seasons. *Remote Sens.* 2018;10:366.
- [37] Rivaro P, Ianni C, Langone L, et al. Physical and biological forcing of mesoscale variability in the carbonate system of the Ross Sea (Antarctica) during summer 2014. *J Mar Syst.* 2017;166:144–158.
- [38] Misić C, Covazzi Harriague A, Mangoni O, et al. Effects of physical constraints on the lability of POM during summer in the Ross Sea. *J Mar Syst.* 2017;166:132–143.
- [39] Grotti M, Soggia F, Ardini F, et al. Determination of sub-nanomolar levels of iron in sea-water using reaction cell inductively coupled plasma mass spectrometry after Mg(OH)<sub>2</sub> coprecipitation. *J Anal At Spectrom.* 2009;24:522–527.
- [40] Wu JF, Boyle EA. Determination of iron in seawater by high-resolution isotope dilution inductively coupled plasma mass spectrometry after Mg(OH)<sub>2</sub> coprecipitation. *Anal Chim Acta.* 1998;367:183–191.
- [41] Tanner SD, Baranov VI, Vollkopf U. A dynamic reaction cell for inductively coupled plasma mass spectrometry (ICP-DRC-MS) – Part III. Optimization and analytical performance. *J Anal At Spectrom.* 2000;15:1261–1269.
- [42] Vieira MA, Welz B, Curtius AJ. Determination of arsenic in sediments, coal and fly ash slurries after ultrasonic treatment by hydride generation atomic absorption spectrometry and trapping in an iridium-treated graphite tube. *Spectrochim Acta Part B-At Spectrosc.* 2002;57:2057–2067.
- [43] van den Berg CMG. Chemical speciation of iron in seawater by cathodic stripping voltammetry with dihydroxynaphthalene. *Anal Chem.* 2006;78:156–163.
- [44] Laglera LM, Battaglia G, Van den Berg CMG. Effect of humic substances on the iron speciation in natural waters by CLE/CSV. *Mar Chem.* 2011;127:134–143.
- [45] Ružić I. Theoretical aspects of the direct titration of natural waters and its information yield for trace metal speciation. *Anal Chim Acta.* 1982;140:99–113.
- [46] Van Den Berg CMG. Determination of copper complexation with natural organic ligands in seawater by equilibration with MnO<sub>2</sub>. I. Theory *Mar Chem.* 1982;11:307–322.
- [47] Turoczy NJ, Sherwood JE. Modification of the van den Berg/Ruzic method for the investigation of complexation parameters of natural waters. *Anal Chim Acta.* 1997;354:15–21.
- [48] Gerringa LJA, Rijkenberg MJA, Thuróczy C-E, et al. A critical look at the calculation of the binding characteristics and concentration of iron complexing ligands in seawater with suggested improvements. *Environ Chem.* 2014;11:114–136.
- [49] Hudson RJM, Covault DT, Morel FMM. Investigations of iron coordination and redox reactions in seawater using <sup>59</sup>Fe radiometry and ion-pair solvent extraction of amphiphilic iron complexes. *Mar Chem.* 1992;38:209–235.
- [50] Thuróczy CE, Gerringa LJA, Klunder MB, et al. Observation of consistent trends in the organic complexation of dissolved iron in the Atlantic sector of the Southern Ocean. *Deep Sea Res Part II Top Stud Oceanogr.* 2011;58:2695–2706.

- [51] Calace N, Casagrande A, Mirante S, et al. Distribution of humic substances dissolved and particulated in water column in Ross Sea, Antarctica. *Microchem J.* 2010;96:218–224.
- [52] Grasshoff K. Determination of oxygen. In: Grasshoff K, Ehrhardt M, Kremling K, editor. *Methods Seawater Analysis*. Weinheim: Verlag Chemie; 1983. p. 61–72.
- [53] Hansen HP, Grasshoff K. Automated chemical analysis. In: Grasshoff K, Ehrhardt M, Kremling K, editor. *Methods Seawater Analysis*. Weinheim: Verlag Chemie; 1983. p. 347–370.
- [54] Celussi M, Malfatti F, Franzo A, et al. Ocean acidification effect on prokaryotic metabolism tested in two diverse trophic regimes in the Mediterranean Sea. *Estuar Coast Shelf Sci.* 2017;186:125–138.
- [55] Lee S, Fuhrman JA. Relationships between biovolume and biomass of naturally derived marine bacterioplankton. *Appl Environ Microbiol.* 1987;53:1298–1303.
- [56] Wunsch C. *Modern observational physical oceanography: understanding the global ocean*. Princeton (NJ): Princeton University Press; 2015.
- [57] Schlitzerp R. Ocean data view [Internet]. 2015. Available from: <http://odv.awi.de/>.
- [58] Budillon G, Pacciaroni M, Cozzi S, et al. An optimum multiparameter mixing analysis of the shelf waters in the Ross Sea. *Antarct Sci.* 2003;15:105–118.
- [59] Massolo S, Messa R, Rivaro P, et al. Annual and spatial variations of chemical and physical properties in the Ross Sea surface waters (Antarctica). *Cont Shelf Res.* 2009;29:2333–2344.
- [60] Martin JH, Gordon RM, Fitzwater SE. Iron in Antarctic waters. *Nature.* 1990;345:156–158.
- [61] Rivaro P, Ianni C, Massolo S, et al. Distribution of dissolved labile and particulate iron and copper in Terra Nova Bay polynya (Ross Sea, Antarctica) surface waters in relation to nutrients and phytoplankton growth. *Cont Shelf Res.* 2011;31:879–889.
- [62] Annett AL, Skiba M, Henley SF, et al. Comparative roles of upwelling and glacial iron sources in Ryder Bay, coastal western Antarctic Peninsula. *Mar Chem.* 2015;176:21–33.
- [63] Quéroué F, Sarthou G, Planquette HF, et al. High variability in dissolved iron concentrations in the vicinity of the Kerguelen Islands (Southern Ocean). *Biogeosciences.* 2015;12:3869–3883.
- [64] Ibsanmi E, Sander SG, Boyd PW, et al. Vertical distributions of iron-(III) complexing ligands in the Southern Ocean. *Deep Sea Res Part II Top Stud Oceanogr.* 2011;58:2113–2125.
- [65] Thuróczy C-E, Alderkamp A-C, Laan P, et al. Key role of organic complexation of iron in sustaining phytoplankton blooms in the Pine Island and Amundsen Polynyas (Southern Ocean). *Deep Sea Res Part II Top Stud Oceanogr.* 2012; 71–76:49–60.
- [66] Nolting RF, Gerringa LJA, Swagerman MJW, et al. Fe (III) speciation in the high nutrient, low chlorophyll Pacific region of the Southern Ocean. *Mar Chem.* 1998;62:335–352.
- [67] McGillicuddy DJ, Budillon G, Kustka A. Mesoscale and high-frequency variability in the Ross Sea (Antarctica): an introduction to the special issue. *J Mar Syst.* 2017;166:1–3.
- [68] Wang S, Bailey D, Lindsay K, et al. Impact of sea ice on the marine iron cycle and phytoplankton productivity. *Biogeosciences.* 2014;11:4713–4731.
- [69] Parkhill JP, Maillet G, Cullen JJ. Fluorescence-based maximal quantum yield for PSII as a diagnostic of nutrient stress. *J Phycol.* 2001;37:517–529.
- [70] Croot PL, Andersson K, Öztürk M, et al. The distribution and speciation of iron along 6°E in the Southern Ocean. *Deep Sea Res Part II Top Stud Oceanogr.* 2004;51:2857–2879.
- [71] Gerringa LJA, Blain S, Laan P, et al. Fe-binding dissolved organic ligands near the Kerguelen Archipelago in the Southern Ocean (Indian sector). *Deep Sea Res Part II Top Stud Oceanogr.* 2008;55:606–621.
- [72] Hassler CS, van den Berg VD, Boyd PW. Toward a regional classification to provide a more inclusive examination of the ocean biogeochemistry of iron-binding ligands. *Front Mar Sci.* 2017;4:19.
- [73] Lannuzel D, Grotti M, Abelloschi ML, et al. Organic ligands control the concentrations of dissolved iron in Antarctic sea ice. *Mar Chem.* 2015;174:120–130.
- [74] Del Negro P, Crevatin E, Larato C, et al. Mucilage microcosms. *Sci Total Environ.* 2005;353:258–269.
- [75] Delmont TO, Hammar KM, Ducklow HW, et al. Phaeocystis antarctica blooms strongly influence bacterial community structures in the Amundsen Sea polynya. *Front Microbiol.* 2014;5:646.